



## Vacancy-Driven Anisotropic Defect Distribution in the Battery-Cathode Material $\text{LiFePO}_4$

Jaekwang Lee,<sup>1,2</sup> Wu Zhou,<sup>1,2</sup> Juan C. Idrobo,<sup>1,2</sup> Stephen J. Pennycook,<sup>2</sup> and Sokrates T. Pantelides<sup>1,2</sup>

<sup>1</sup>*Department of Physics Astronomy, Vanderbilt University, Nashville, Tennessee 37235, USA*

<sup>2</sup>*Materials Science Technology Division, Oak Ridge National Laboratory, Oak Ridge, Tennessee 37831, USA*

(Received 7 April 2011; revised manuscript received 10 June 2011; published 18 August 2011)

Li-ion mobility in  $\text{LiFePO}_4$ , a key property for energy applications, is impeded by Fe antisite defects ( $\text{Fe}_{\text{Li}}$ ) that form in select  $b$ -axis channels. Here we combine first-principles calculations, statistical mechanics, and scanning transmission electron microscopy to identify the origin of the effect: Li vacancies ( $V_{\text{Li}}$ ) are confined in one-dimensional  $b$ -axis channels, shuttling between neighboring  $\text{Fe}_{\text{Li}}$ . Segregation in select channels results in shorter  $\text{Fe}_{\text{Li}}\text{-Fe}_{\text{Li}}$  spans, whereby the energy is lowered by the  $V_{\text{Li}}$ 's spending more time bound to end-point  $\text{Fe}_{\text{Li}}$ 's.  $V_{\text{Li}}\text{-Fe}_{\text{Li}}\text{-}V_{\text{Li}}$  complexes also form, accounting for observed electron energy loss spectroscopy features.

DOI: [10.1103/PhysRevLett.107.085507](https://doi.org/10.1103/PhysRevLett.107.085507)

PACS numbers: 82.47.Aa, 61.72.Bb, 61.72.Ff, 68.55.Ln

$\text{LiFePO}_4$  is a promising new-generation cathode material for Li rechargeable batteries because of its high energy density, high safety, low cost, and environmental friendliness [1–3]. The Li-ion mobility is the key parameter for battery applications with high energy density. Computational and experimental studies of  $\text{LiFePO}_4$  indicate that  $\text{Li}^+$  ion migration occurs preferentially via one-dimensional channels oriented along the [010] direction ( $b$  axis) [4]. Such one-dimensional diffusion, however, is highly sensitive to the presence of immobile or low-mobility defects in the diffusion path. Even a single immobile defect in the path can block long-range diffusion.

Recently, Chung *et al.* reported that iron antisite defects ( $\text{Fe}_{\text{Li}}$ ) form preferentially in *only a few* channels along the  $b$  axis instead of being homogeneously distributed in the lattice [5]. This kind of segregation is important, because only a few diffusion channels are blocked, leaving most of them available for Li diffusion. The ability to control this segregation is, therefore, necessary in order to maximize the fraction of unblocked diffusion channels and optimize device performance. The cause of the  $\text{Fe}_{\text{Li}}$  segregation, however, remains unknown.

In this Letter, we use first-principles calculations and statistical mechanics to show that the observed segregation of  $\text{Fe}_{\text{Li}}$  defects is the result of an unusual energy-lowering mechanism that is a feature of the one-dimensional nature of the Li diffusion paths. To unveil this mechanism, we need to recognize that the  $b$ -axis channels are one-dimensional arrays of Li ions and that the presence of  $V_{\text{Li}}$  is essential for Li migration. An appropriate concentration of  $V_{\text{Li}}$  is in fact built in during the synthesis of the material. If  $\text{LiFePO}_4$  were a material where Li diffusion could occur in three dimensions, then the  $\text{Fe}_{\text{Li}}$  defects would be randomly distributed. The one-dimensional nature of Li diffusion induces segregation in only a few channels as follows. When a number of  $\text{Fe}_{\text{Li}}$  are present in a channel, the  $V_{\text{Li}}$ 's are confined in segments whose length is equal to the  $\text{Fe}_{\text{Li}}$  spacing.  $V_{\text{Li}}$ 's are then forced to shuttle

between neighboring  $\text{Fe}_{\text{Li}}$ 's, but they also spend time being bound to end-point  $\text{Fe}_{\text{Li}}$ 's. Segregation of  $\text{Fe}_{\text{Li}}$ 's along a few  $b$ -axis channels decreases the mean distance between  $\text{Fe}_{\text{Li}}$ 's, which then increases the time that the  $V_{\text{Li}}$  spend bound to end-point  $\text{Fe}_{\text{Li}}$ 's. The net result is a systematic energy lowering that drives the segregation during the synthesis of the material. Based on a one-dimensional random walk with absorbing boundaries, we derive an analytical expression for the total energy lowering  $E(L)$  as a function of temperature and the average distance  $L$  between neighboring  $\text{Fe}_{\text{Li}}$ 's. Finally, we report new atomically resolved electron energy loss spectroscopy (EELS) obtained with an aberration-corrected scanning transmission electron microscopy. Analysis of the Fe  $L_{2,3}$  edge fine structure reveals that  $\text{Fe}_{\text{Li}}$  in the  $b$ -axis channels has a slightly higher oxidation state relative to the nominal value of +2 for Fe in  $\text{LiFePO}_4$ . This effect can be attributed to the formation of  $V_{\text{Li}}\text{-Fe}_{\text{Li}}\text{-}V_{\text{Li}}$  clusters, which is consistent with the energy-lowering mechanism proposed here: A  $\text{Fe}_{\text{Li}}$  in a  $b$ -axis channel can bind a  $V_{\text{Li}}$  on either side for a fraction of time as the  $V_{\text{Li}}$  shuttle between end-point  $\text{Fe}_{\text{Li}}$ 's.

The calculations were performed by using density functional theory in the generalized gradient approximation and the projector-augmented wave method with a plane-wave basis as implemented in the Vienna *Ab Initio* Simulation package (VASP) code [6]. We used a kinetic energy cutoff of 500 eV, a  $1 \times 2 \times 2$  supercell [Fig. 1(a)] or  $1 \times 3 \times 2$  supercell to accommodate larger defect separations, and a  $6 \times 6 \times 6$  Monkhorst-Pack  $k$ -point mesh centered at the  $\Gamma$  point. We applied a Hubbard  $U$  correction with  $U = 4.3$  eV to describe the Fe- $3d$  states. A  $U_{\text{eff}}$  ( $U$ - $J$ ) value of 4.3 eV was chosen based on the average values for  $\text{Fe}^{2+}$  ( $U_{\text{eff}} = 3.7$  eV in  $\text{LiFePO}_4$ ) and  $\text{Fe}^{3+}$  ( $U_{\text{eff}} = 4.9$  eV for  $\text{FePO}_4$ ) calculated by Zhou *et al.* [7]. Ionic positions were relaxed by using a conjugate gradient minimization until all the forces acting on ions were smaller than 40 meV/Å per ion.

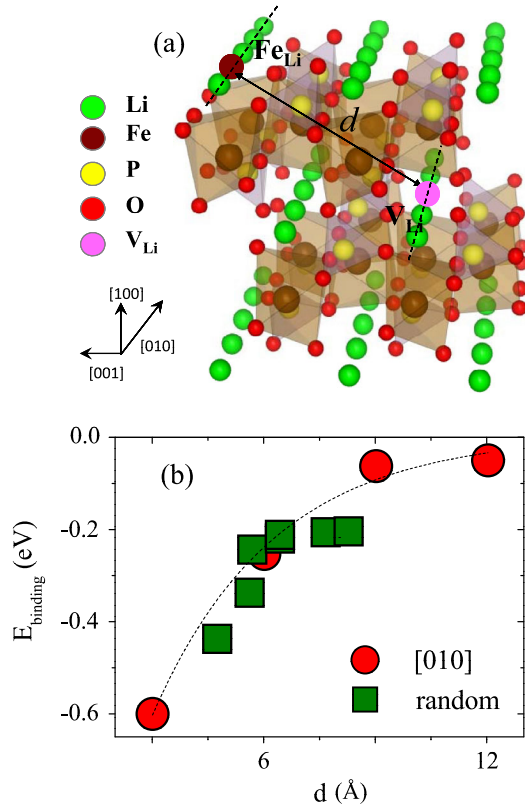


FIG. 1 (color online). (a) Schematic of  $\text{Li}_{14}\text{Fe}_{17}\text{P}_{16}\text{O}_{64}$  including one  $\text{Fe}_{\text{Li}}\text{-V}_{\text{Li}}$  pair separated by a distance  $d$ . (b) Binding energy for  $\text{Fe}_{\text{Li}}\text{-V}_{\text{Li}}$  pairs as a function of separation  $d$ . The red points are for  $\text{Fe}_{\text{Li}}$  and  $\text{V}_{\text{Li}}$  on the same  $b$  axis; green points are for  $\text{Fe}_{\text{Li}}$  and  $\text{V}_{\text{Li}}$  on different  $b$  axes.

We note that prior papers on  $\text{LiFePO}_4$  and similar compounds often refer to antisite defects as being “cation exchange pairs,” e.g.,  $\text{Fe}_{\text{Li}}$  and  $\text{Li}_{\text{Fe}}$  pairs, assessing the energy of their formation by the net cation exchange energy (the two defects can be either far from each other or bound in close proximity) [5,8,9]. However, the concentrations of  $\text{Fe}_{\text{Li}}$  and  $\text{Li}_{\text{Fe}}$  are in fact independent and, in equilibrium, are governed by the respective formation energies, which depend on the chemical potentials of pertinent species (see, e.g., Ref. [10]). In turn, the chemical potentials depend on the growth conditions, i.e., the nature of the Fe and Li sources (reservoirs). In a similar way, prior papers assign a nominal charge to defects corresponding to the “oxidation state,” which is *not* a physical charge [11]. The actual charge states of defects are in fact controlled by the Fermi energy, which in turn is controlled by other means, e.g., doping. Consequently, the formation energies of charged defects are also functions of the electron chemical potential, namely, the Fermi energy [10]. Concentrations of defects can of course have nonequilibrium values, controlled by kinetic constraints during growth. In the present work we consider  $\text{Fe}_{\text{Li}}$  defects in  $\text{LiFePO}_4$ , which have been observed by electron microscopy (see Fig. 4 and Refs. [5,12]). The presence of  $\text{Li}_{\text{Fe}}$

defects is not relevant to the scope of this Letter. Similarly,  $\text{V}_{\text{Li}}$ ’s are typically viewed together with Li interstitials as “Frenkel pairs” [8,9], but the concentrations of the two defects are in fact independent. We will be concerned only with  $\text{V}_{\text{Li}}$ ’s, which are known to form during synthesis [8] and are indispensable for Li diffusion.

In order to investigate the effect of  $\text{V}_{\text{Li}}$ ’s on the aggregation of  $\text{Fe}_{\text{Li}}$  defects, we calculated the binding energy between a  $\text{Fe}_{\text{Li}}$  in a  $b$ -axis channel and a  $\text{V}_{\text{Li}}$  separated by a distance  $d$ . The binding energy is defined by  $E_b = E_{\text{Fe}_{\text{Li}}\text{-V}_{\text{Li}}} - (E_{\text{Fe}_{\text{Li}}} + E_{\text{V}_{\text{Li}}})/2$ , where  $E_{\text{Fe}_{\text{Li}}\text{-V}_{\text{Li}}}$ ,  $E_{\text{Fe}_{\text{Li}}}$ , and  $E_{\text{V}_{\text{Li}}}$  are the total energies of supercells containing a  $\text{Fe}_{\text{Li}}\text{-V}_{\text{Li}}$  bound pair, a  $\text{Fe}_{\text{Li}}$ , and a  $\text{V}_{\text{Li}}$ , respectively. The results are shown in Fig. 1(b). The zero of energy corresponds to infinite separation between the two defects. The red points correspond to the  $\text{V}_{\text{Li}}$  being in the same  $b$ -axis channel with the  $\text{Fe}_{\text{Li}}$ . The green points correspond to the  $\text{V}_{\text{Li}}$  being in a different channel. As expected, the largest binding energy, 0.6 eV, is for the nearest-neighbor pair along the  $b$ -axis channel ( $d \sim 3$  Å). This value is in agreement with previous estimates based on classical potentials [8,9]. We note that the binding energy displays a Coulombic dependence  $d^{-1}$  on the separation distance  $d$ , suggesting that the two defects in a neutral supercell carry opposite charges (as noted earlier, the values of these charges are in principle controlled by the Fermi energy, which in turn can be controlled by other means, e.g., doping; the results here indicate that, in a neutral, undoped supercell, the Fermi level lies between energy levels belonging to the two defects so that an electron exchange occurs, leading to Coulombic attraction).

So far, we have shown that  $\text{Fe}_{\text{Li}}$ ’s in  $b$ -axis channels are likely to have a  $\text{V}_{\text{Li}}$  adjacent to them along the same channel. In order to explain the aggregation of  $\text{Fe}_{\text{Li}}$ ’s only in a select few  $b$ -axis channels, we now consider the fact that Li diffusion in olivine  $\text{LiFePO}_4$  is one-dimensional along the  $b$ -axis channels. We have verified, by using the nudged-elastic-band method [13], that the migration barrier for a  $\text{V}_{\text{Li}}$  along the  $b$ -axis channel is in fact lowest by far, with a value of 0.5 eV, in good agreement with prior results [8,14]. The key point now is what happens when more than one  $\text{Fe}_{\text{Li}}$  are present in the same channel: A  $\text{V}_{\text{Li}}$  that happens to be between two  $\text{Fe}_{\text{Li}}$ ’s in the same  $b$ -axis channel can shuttle between the two end points of the segment, possibly bind at either end, then be released again, and shuttle until it gets bound again to one of the end points. The potential seen by a  $\text{V}_{\text{Li}}$  in such a segment is shown in Fig. 2(a). Intuitively, we can expect that in shorter segments the  $\text{V}_{\text{Li}}$  will bind more frequently and overall spend more time being bound than free. Segregation of the  $\text{Fe}_{\text{Li}}$  in just a few  $b$ -axis channels produces shorter segments between adjacent  $\text{Fe}_{\text{Li}}$  and hence more time when  $\text{V}_{\text{Li}}$ ’s are bound. This is the source of energy lowering that produces the observed segregation. It is clearly a feature of the one-dimensional nature of Li diffusion.

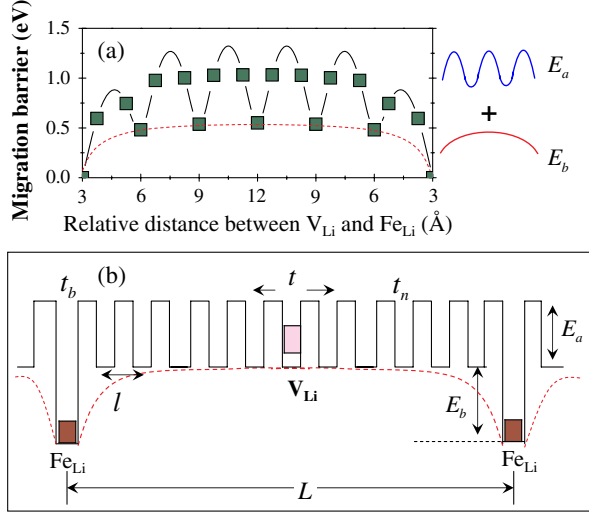


FIG. 2 (color online). (a) Energy landscape for a  $V_{Li}$  shuttling between two  $Fe_{Li}$ 's in a  $b$ -axis channel combining migration barrier and binding energy variation. (b) Schematic version of the same figure, defining a one-dimensional random walk with absorbing end points. The symbols are defined in the text.

In order to quantify the above effect, we map the shuttling of the  $V_{Li}$  between two  $Fe_{Li}$ 's on a one-dimensional random walk [15,16] as illustrated in Fig. 2(b). We define the *energy lowering* arising from a single segment containing a single  $V_{Li}$  to be proportional to the ratio of the time  $t_b$  that a  $V_{Li}$  spends bound to an end-point  $Fe_{Li}$  to the sum of  $t_b$  and the time  $t$  that a  $V_{Li}$  spends shuttling prior to being bound:

$$E = \frac{t_b}{t + t_b} E_b. \quad (1)$$

In the case of an absorbing boundary,  $t$  is approximately given by [15–17]

$$t \simeq \frac{N^2}{4} t_n = \frac{L^2}{4l^2} t_n, \quad (2)$$

where  $t_n$  is the time of a single migration jump of length  $l$  as shown in Fig. 2(b). According to transition state theory [18],

$$t_n = \nu^{-1} \exp\left(\frac{E_a}{k_B T}\right), \quad (3)$$

where  $\nu$  is the characteristic attempt frequency and  $E_a$  is the  $V_{Li}$  migration energy. Near the boundary,  $V_{Li}$  is attracted and can be bound with binding energy  $E_b$ , whereby  $t_b$  is given by

$$t_b = \nu^{-1} \exp\left(\frac{E_a + |E_b|}{k_B T}\right) = \exp\left(\frac{|E_b|}{k_B T}\right) t_n. \quad (4)$$

We then have

$$\frac{t}{t_b} = \frac{L^2}{4l^2 \exp\left(\frac{|E_b|}{k_B T}\right)}. \quad (5)$$

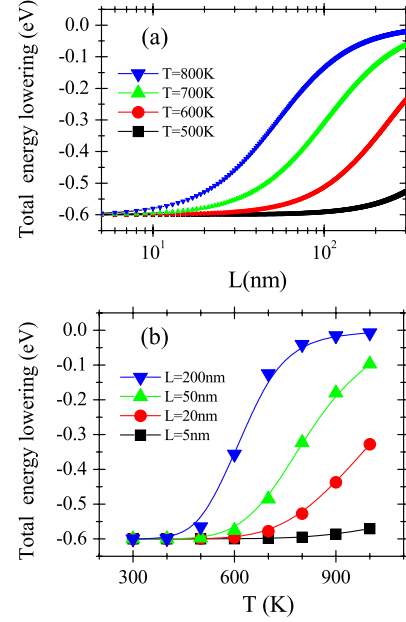


FIG. 3 (color online). Total energy lowering (a) as a function of separation  $L$  between  $Fe_{Li}$ 's and (b) as a function of temperature  $T$ .

Consequently, the total energy lowering  $E$  can be expressed as a function of the distance  $L$  between two  $Fe_{Li}$  defects:

$$E(L) = \frac{E_b}{1 + \left(\frac{L}{b_0}\right)^2 \exp\left(-\frac{|E_b|}{k_B T}\right)}. \quad (6)$$

Here  $b_0$  is the interatomic spacing of Li atoms along the  $b$  axis,  $k_B$  is the Boltzmann constant, and  $T$  is the temperature at which the diffusion of  $V_{Li}$  occurs (synthesis temperature). The energy lowering  $E(L)$  is plotted in Fig. 3 as a function of  $L$  and as a function of  $T$ . Figure 3(a) shows that, for each temperature at which the synthesis occurs, shorter segments mean lower energy, which is the driving force of the observed segregation of  $Fe_{Li}$ 's in only a few  $b$ -axis channels. The process is of course ultimately limited by kinetic constraints. The message of the figure, however, is that a lower synthesis temperature favors the desirable segregation, but a lower temperature also means that kinetic constraints are more effective in limiting the segregation. Extended annealing at a relatively low temperature, smaller than 600 K, can be most effective in producing increased segregation. These results explain why  $Fe_{Li}$ 's are present if the samples are synthesized at temperatures lower than 200 °C [19,20] or when the samples are annealed at 600 °C [12], whereas  $Fe_{Li}$ 's are scarcely observed when the samples are annealed at 800 °C [12].

So far, we considered only the case of individual segments with a single  $V_{Li}$  between two  $Fe_{Li}$ 's. The case of more than one  $V_{Li}$  in a segment can in principle be treated, but the results are not expected to change significantly as  $V_{Li}$ 's are indistinguishable. When we consider multiple



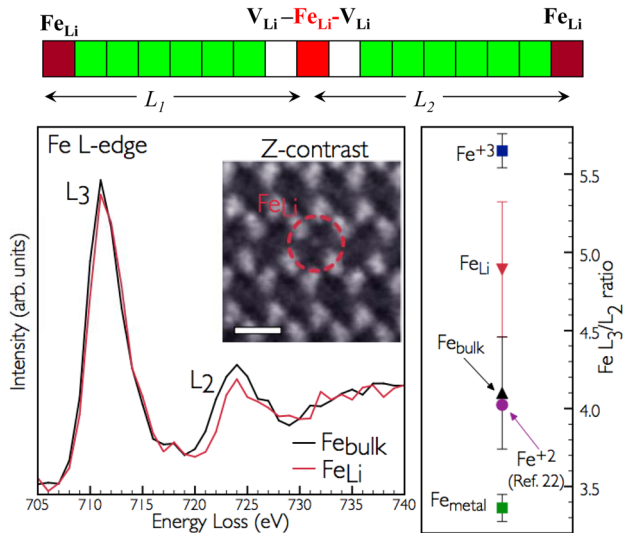


FIG. 4 (color online). Top: Schematic figure of the probable configuration of  $Fe_{Li}$  with a higher Fe oxidation state. Bottom: (Left) EELS data of  $Fe_{Li}$  (shown in the red circle in the inset) and of Fe in bulk positions in  $LiFePO_4$ . The inset shows an atomically resolved Z-contrast image of  $LiFePO_4$  oriented along the *b* axis. The scale bar is 0.5 nm. (Right) Fe  $L_3/L_2$  ratios for  $Fe_{Li}$  (red triangle) and  $Fe_{bulk}$  (black triangle) sites of  $LiFePO_4$  compared with different iron compounds.  $Fe^{+3}$  and  $Fe_{metal}$  correspond to spectra obtained for  $\alpha$ - $Fe_2O_3$  and metallic iron thin film, respectively. The data point shown as a purple circle corresponds to the Fe  $L_3/L_2$  ratio of the FeO spectra, i.e.,  $Fe^{+2}$ , presented in Ref. [22] and calculated by using the second derivative method of Ref. [23]. The data point is shown only for comparison purposes.

segments, we recognize the possibility that  $V_{Li}-Fe_{Li}-V_{Li}$  complexes can form, as shown in Fig. 4. Clearly, the shorter the segments are, which lowers the energy of the system, the higher the probability of forming these complexes. We will now present experimental evidence that such complexes in fact exist.

To investigate the presence of  $V_{Li}-Fe_{Li}-V_{Li}$  complexes, we obtained atomic-resolution EELS in a  $LiFePO_4$  sample by using an aberration-corrected Nion UltraSTEM [21] at 100 kV operating voltage. The convergence semiangle for the incident probe was 31 mrad, with an EELS collection semiangle of 48 mrad, both of which are confirmed to effectively eliminate any effects of crystal anisotropy for bulk Fe. An acquisition time of 0.2 s per spectrum and an energy dispersion of 1 eV per channel were used. The Fe *L*-edge spectra (background subtracted) shown in Fig. 4 are the result of the sum of 8 and 10 individual spectra for  $Fe_{Li}$  and of Fe in bulk positions in  $LiFePO_4$ , respectively. It is well accepted that the ratio between the  $L_3$  and  $L_2$  peak can be used as an indication of the oxidation state, with a larger  $L_3/L_2$  ratio corresponding to a higher Fe valence [22]. We find that the Fe  $L_3/L_2$  ratio (calculated by using the second derivative method [23]) for the  $Fe_{Li}$  is 18% larger than that for the Fe in the bulk position. This

qualitatively indicates that the oxidation state of Fe at the antisite position is higher than the average oxidation state of Fe in the bulk  $LiFePO_4$  material (i.e., +2). Indeed, the nominal Fe oxidation state in  $Fe_{Li}$  is +1, in  $Fe_{Li}-V_{Li}$  it is +2, and in  $V_{Li}-Fe_{Li}-V_{Li}$  it is +3, whereby the presence of  $V_{Li}-Fe_{Li}-V_{Li}$  accounts for the observed Fe oxidation state higher than +2. A comparison of the Fe  $L_3/L_2$  ratios of a  $Fe_{Li}$  site with respect to a  $Fe_{bulk}$  site of  $LiFePO_4$  and other iron compounds is also shown in Fig. 4.

In conclusion, we showed that the observed segregation of  $Fe_{Li}$ 's defects in selective *b* channels is the result of an unusual energy-lowering mechanism that is a feature of the one-dimensional nature of the Li diffusion path.  $V_{Li}$ 's shuttle between  $Fe_{Li}$ 's defects and bind occasionally at the end points along the *b* channels. Segregation of  $Fe_{Li}$ 's in just a few channels results in shorter  $Fe_{Li}-Fe_{Li}$  separations, which induce longer binding times, lowering the system's energy. The analysis suggests temperatures for growth and/or annealing to optimize segregation and maximize Li diffusion.

We thank Dr. Nancy Dudney, who supplied the  $LiFePO_4$  sample for EELS measurement. This research was partially supported by the National Science Foundation under Grant No. DMR-0938330 (J. C. I. and W. Z.), by ORNL's Shared Research Equipment (SHaRE) User Facility, which is sponsored by the Office of Basic Energy Sciences, U.S. Department of Energy (J. C. I.) and the Office of Basic Energy Sciences, Materials Sciences and Engineering Division, U.S. Department of Energy (S. J. P., J. L., and S. T. P.), DOE Grant No. DE-FG02-09ER46554 (S. T. P.), and by the McMinn Endowment (S. T. P.) at Vanderbilt University. This research used resources of the National Energy Research Scientific Computing Center, which is supported by the Office of Science of the U.S. Department of Energy under Contract No. DE-AC02-05CH11231.

- [1] A. K. Padhi *et al.*, *J. Electrochem. Soc.* **144**, 1188 (1997).
- [2] B. L. Ellis *et al.*, *Chem. Mater.* **22**, 691 (2010).
- [3] S. Nishimura *et al.*, *Nature Mater.* **7**, 707 (2008).
- [4] C. Quyang *et al.*, *Phys. Rev. B* **69**, 104303 (2004).
- [5] S.-Y. Chung *et al.*, *Angew. Chem., Int. Ed.* **48**, 543 (2009).
- [6] G. Kresse *et al.*, *Comput. Mater. Sci.* **6**, 15 (1996).
- [7] F. Zhou *et al.*, *Electrochem. Comm.* **6**, 1144 (2004).
- [8] M. S. Islam *et al.*, *Chem. Mater.* **17**, 5085 (2005).
- [9] C. A. Fisher *et al.*, *Chem. Mater.* **20**, 5907 (2008).
- [10] D. B. Laks *et al.*, *Phys. Rev. B* **45**, 10965 (1992).
- [11] W. Luo *et al.*, *Phys. Rev. Lett.* **99**, 036402 (2007).
- [12] S.-Y. Chung *et al.*, *Phys. Rev. Lett.* **100**, 125502 (2008).
- [13] G. Mills *et al.*, *Surf. Sci.* **324**, 305 (1995).
- [14] D. Morgan *et al.*, *Electrochem. Solid-State Lett.* **7**, A30 (2004).
- [15] M. A. El-Shehawy, *J. Phys. A* **33**, 9005 (2000).
- [16] M. A. El-Shehawy, *SIAM J. Matrix Anal. Appl.* **30**, 497 (2008).

- [17] The full expression is  $t = (\frac{N^2}{4} + N \frac{1-\beta}{\beta})t_n$ , where  $\beta$ , the absorption probability, is given by  $\beta \approx 1 - \frac{t_n}{t_b} = 1 - \exp(-\frac{|E_b|}{k_B T}) \approx 1$ .
- [18] G. H. Vineyard, *J. Phys. Chem. Solids* **3**, 121 (1957).
- [19] J. Chen *et al.*, *Electrochem. Commun.* **8**, 855 (2006).
- [20] S. Yang *et al.*, *Electrochem. Commun.* **4**, 239 (2002).
- [21] O. L. Krivanek *et al.*, *Ultramicroscopy* **110**, 935 (2010).
- [22] C. Colliex, T. Manoubi, and C. Ortiz, *Phys. Rev. B* **44**, 11 402 (1991).
- [23] G. A. Botton *et al.*, *J. Microsc.* **180**, 211 (1995).